

# COMPARISON OF LOW-ENERGY LUNAR TRANSFER TRAJECTORIES TO INVARIANT MANIFOLDS

Rodney L. Anderson\* and Jeffrey S. Parker\*

In this study, transfer trajectories from the Earth to the Moon that encounter the Moon at various flight path angles are examined, and lunar approach trajectories are compared to the invariant manifolds of selected unstable orbits in the circular restricted three-body problem. Previous work focused on lunar impact and landing trajectories encountering the Moon normal to the surface, and this research extends the problem with different flight path angles in three dimensions. The lunar landing geometry for a range of Jacobi constants are computed, and approaches to the Moon via invariant manifolds from unstable orbits are analyzed for different energy levels.

## INTRODUCTION

The design of Earth-Moon transfer trajectories is a problem with a rich heritage that has been approached with a wide variety of techniques. These techniques in combination with ever-changing mission requirements have produced an even greater number of possible trajectories ranging from the direct trajectories of Apollo<sup>1</sup> to more indirect trajectories making heavy use of multi-body dynamics. In addition to transfers to lunar orbit or the lunar surface, many previous conceptual mission designs have included the use of libration point orbits in the three-body problem for use in transfer to the Moon or to achieve operational orbits around the Moon. Now, the first mission to operationally fly on a lunar libration orbit, ARTEMIS,<sup>2,3</sup> has successfully demonstrated the feasibility of lunar libration orbit trajectories, and the two planned GRAIL<sup>4-6</sup> spacecraft will follow low-energy trajectories as part of their mission. With the increased use of these types of trajectories in mission design, it becomes important to examine the possible connections between unstable libration orbits and other locations of importance such as the lunar surface. Often the trajectories of interest are not those that travel directly to the unstable orbits, rather they are guided by the invariant manifolds of the unstable three-body orbits. Using the invariant manifolds as guides for potential trajectories provides mission designers a method for reducing the complications involved with design in this highly nonlinear dynamical environment. This work seeks to place low-energy lunar transfers to the surface in context with these invariant manifolds to enable mission designers to more easily develop trajectories in this multi-body environment.

Some framework and understanding already exists in regard to the relationship between invariant manifolds of unstable orbits and the Moon. Much of the work to design low-energy trajectories from the Earth to the Moon has focused on the use of libration point orbits along with their stable and unstable manifolds.<sup>7-10</sup> Koon, Lo, Marsden, and Ross examined this problem for the planar case,<sup>11</sup> and Parker studied approach cases to lunar libration orbits using invariant manifolds in his dissertation.<sup>12</sup> Baoyin and McInnes analyzed some specific cases of transfers from libration points and planar Lyapunov orbits to the lunar surface.<sup>13</sup> In particular, they searched for the Jacobi constant that would provide complete coverage of the lunar surface by the invariant manifolds of the selected Lyapunov orbit. Kirchbach et al.<sup>14</sup> looked at the characteristics of the invariant manifolds of a Lyapunov orbit as they intersected the surface of Europa in the context of the escape problem. Alessi, Gómez, and Masdemont<sup>15</sup> examined the locations of the Moon reachable by

\*Member of Technical Staff, Jet Propulsion Laboratory, California Institute of Technology, 4800 Oak Grove Drive, M/S 301-121, Pasadena, CA 91109

© 2011 California Institute of Technology. Government sponsorship acknowledged.

the stable manifolds of a range of halo orbits and square Lissajous orbits. They computed the intersections of these invariant manifolds with the surface of the Moon with the expectation that they could be used for astronauts to escape to a libration point orbit if necessary.

In this work, we explore unstable orbits along with their invariant manifolds and examine the computed lunar approach trajectories within the context of the resulting invariant manifold pathways. It has been known since Conley's research<sup>16</sup> that libration orbits act as a gateway through which transiting trajectories must pass for certain energies. The specific details of how these transiting trajectories behave as they approach the Moon relative to the invariant manifolds are of interest here. A focus of this study is the exploration of the practical aspects and implications of this knowledge in the Earth-Moon system for mission design applications. In our previous work,<sup>17</sup> we examined Earth-Moon ballistic transfer trajectories to the lunar surface with trajectories impacting the Moon at varying angles for the planar case and normal to the surface for collision orbits<sup>18,19</sup> in the three-dimensional case. These results for trajectories encountering the Moon normal to the surface were obtained using techniques previously implemented in Anderson and Lo.<sup>20</sup> This analysis is extended here to examine three-dimensional cases with additional flight path angles at the lunar surface. Next, the invariant manifolds of selected unstable orbits in the circular restricted three-body problem (CRTBP) are computed for different Jacobi constants, and their approach characteristics at the Moon are analyzed. These invariant manifolds are then compared to the previously computed trajectories and used to provide a context for these lunar approach trajectories.

## MODELS

The analyses in this study are carried out within both the CRTBP and the ephemeris problem. The CRTBP generally provides a good approximation to the ephemeris problem, and a variety of tools and symmetries exist within this problem that make it convenient for initial analysis. While trajectories similar to those that exist within the CRTBP generally exist within the ephemeris problem, it does not necessarily capture all those trajectories that exist in the ephemeris problem as the result of perturbations of additional bodies.<sup>17</sup> The ephemeris model is therefore used in the analysis to include these additional trajectories that are especially important in the low-energy regime.

### Circular Restricted Three-Body Problem

Many of the trajectories and periodic orbits used in this analysis are computed in the CRTBP.<sup>21</sup> In this model, a larger body (the primary) and a smaller body (the secondary) are assumed to rotate about their center of mass in circular orbits, and the motion of a third infinitesimal mass is modeled in this system. The equations of motion are formulated in a rotating frame where the  $x$  axis is aligned with the position of the primary and secondary, and the positive  $x$  axis direction is defined in the direction from the primary to the secondary. Dimensionless quantities are used so that the primary has mass  $1 - \mu$ , and the secondary has mass  $\mu$ . The value for  $\mu$  is defined by  $\mu = m_2/(m_1 + m_2)$  where  $m_1$  is the mass of the primary, and  $m_2$  is the mass of the secondary. The distance between the primary and the secondary, the mean motion, and the gravitational constant are all unity. The primary is located at  $x_1 = -\mu$ , and the secondary is located at  $x_2 = 1 - \mu$ . The equations of motion in the rotating frame may be written as

$$\begin{aligned}\ddot{x} - 2\dot{y} &= \frac{\partial \Omega}{\partial x} \\ \ddot{y} + 2\dot{x} &= \frac{\partial \Omega}{\partial y} \\ \ddot{z} &= \frac{\partial \Omega}{\partial z}\end{aligned}\tag{1}$$

where

$$\Omega = \frac{x^2 + y^2}{2} + \frac{(1 - \mu)}{r_1} + \frac{\mu}{r_2}\tag{2}$$

and

$$\begin{aligned} r_1 &= \sqrt{(x - x_1)^2 + y^2 + z^2} \\ r_2 &= \sqrt{(x - x_2)^2 + y^2 + z^2}. \end{aligned} \quad (3)$$

A constant of motion referred to as the Jacobi constant is defined by

$$C = x^2 + y^2 + \frac{2(1 - \mu)}{r_1} + \frac{2\mu}{r_2} - \dot{x}^2 - \dot{y}^2 - \dot{z}^2. \quad (4)$$

For particular values of the Jacobi constant, certain regions, known as forbidden regions, exist where the infinitesimal mass may not travel. Five equilibrium points, referred to as Lagrange points, exist in the CRTBP. The two Lagrange points primarily used in this study are  $L_1$  and  $L_2$  where  $L_1$  exists on the line between the primary and the secondary, and  $L_2$  is on the far side of the secondary from the primary. Various types of unstable periodic orbits, several of which are computed in this study, are known to exist around these points. A useful symmetry is also known to exist in the CRTBP which extends the results of this analysis to other trajectories. Using this symmetry, it is known that if  $(x, y, z, \dot{x}, \dot{y}, \dot{z}, t)$  is a solution in the CRTBP, then  $(x, -y, z, -\dot{x}, \dot{y}, -\dot{z}, -t)$  is also a solution. Given this information, if a trajectory is reflected about the  $x$ - $z$  plane, a valid trajectory may then be obtained by traveling reverse in time. Approach trajectories to the Moon may then be computed from departure trajectories and vice versa. An additional symmetry that will be useful to reduce the amount of computations required for some of the spatial analyses in the CRTBP also exists. For this symmetry, if  $(x, y, z, \dot{x}, \dot{y}, \dot{z}, t)$  is known to exist, then  $(x, y, -z, \dot{x}, \dot{y}, -\dot{z}, t)$  is also a solution. See Miele<sup>22</sup> or Szebehely<sup>21</sup> for more detailed information on these symmetries. The constants used in this model and the rest of the analysis are listed in Table 1. Several useful Jacobi constants, including those computed at the Earth-Moon Lagrange points, are listed here to place the results presented later in the paper in context.

$$\begin{aligned} C_{L_1} &= 3.1883411054012485 \\ C_{L_2} &= 3.1721604503998044 \\ C_{L_3} &= 3.0121471493422489 \\ C_{L_4}, C_{L_5} &= 2.9879970524275450 \\ C_{Avg(L_1, L_2)} &= (C_{L_1} + C_{L_2})/2 = 3.1802507779005262 \end{aligned} \quad (5)$$

**Table 1. Constants used in the CRTBP and this analysis.**

Quantity	Value
$GM_{Earth}$ (km <sup>3</sup> /s <sup>2</sup> )	398600.43623333969
$GM_{Moon}$ (km <sup>3</sup> /s <sup>2</sup> )	4902.80007622774
$\mu$	0.012150584270572
Radius <sub>Earth</sub> (km)	1737.40
Radius <sub>Moon</sub> (km)	6378.14
Period <sub>Moon</sub> (sec.)	2360591.5104

## Invariant Manifolds

Invariant manifolds of unstable orbits play an integral role in many trajectory options for transfers to the lunar surface, and their computation is essential for the comparisons described in this work. They may be computed for a variety of different orbit types, but the focus here is on computing the stable ( $W^s$ ) and unstable ( $W^u$ ) invariant manifolds of libration point orbits about the  $L_1$  and  $L_2$  libration points including Lyapunov and halo orbits. It is well known that these libration orbits act as a gateway through which trajectories transiting between different regions in the low-energy regime in the CRTBP must pass.<sup>16</sup> It is therefore expected that they will serve as guides to further understand these transiting trajectories.

Stable (unstable) manifolds of an unstable periodic orbit may be described as those trajectories that approach the selected orbit as time approaches  $\infty$  ( $-\infty$ ). They are computed by integrating the state transition matrix for one complete period of the orbit (called the monodromy matrix) and examining the stability characteristics of this matrix. The local unstable (stable) direction may be computed from the eigenvector of the eigenvalue with a magnitude greater (less) than one. The stable (unstable) manifolds may be globalized by taking offsets of approximately  $10^{-6}$  in the direction of the desired eigenvector for each point along the orbit and integrating backward (forward) for a selected period of time.<sup>23</sup>

### Ephemeris Model

While the CRTBP is conceptually useful for understanding trajectories in three-body systems and it provides an accurate tool for the initial design of trajectories, the design of real-world trajectories eventually must incorporate accurate information about the position of all bodies from the ephemeris model. For this investigation, the precise orbital characteristics of the Moon are taken into account as well as perturbations from the Sun. The Moon's orbit varies from the assumptions of the CRTBP in that its mean inclination relative to the ecliptic is  $5.145396^\circ$ , and its mean eccentricity is 0.05490.<sup>24</sup> The Moon's mean distance from the Earth is approximately  $3.844 \times 10^5$  km, and it varies from about 363296.44 km to 405503.56 km.<sup>24</sup> The specific ephemeris model chosen for use in this study is the JPL DE421 Planetary and Lunar Ephemerides.<sup>25</sup> More detailed information on lunar constants and the geometry related to the JPL Lunar Ephemeris 403 may be found by referring to Roncoli.<sup>26</sup> For this analysis, only the Sun, Earth, and Moon are included in the integrations, and each of these bodies are modeled as point masses.

### PLANAR ANALYSIS

In our previous work, lunar impact trajectories encountering the lunar surface at a variety of flight path angles were examined to determine their origin given a 200 day integration backward in time. A chaotic set of points were computed that generally formed in bands based on the origin of the trajectory with some structure observed in each band. Results were plotted for different Jacobi constants using the coordinates  $\alpha$

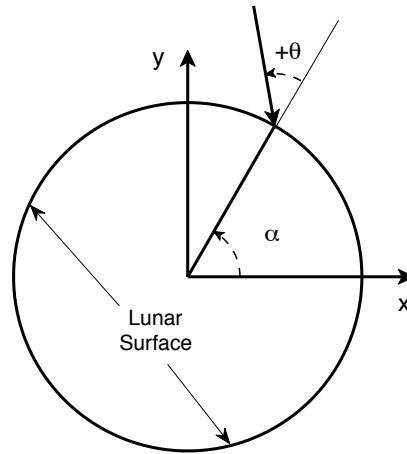


**Figure 1. Diagram showing location and orientation of velocity vector as it intersects the lunar surface. The  $xy$  axes shown here are centered on the Moon in the same orientation as the axes in the rotating frame.**

and  $\theta$  as illustrated in Figure 1. The variable  $\alpha$  corresponds to the location of the impacting trajectory on the surface of the Moon, and  $\theta$  corresponds to the angle of the impacting trajectory with  $0^\circ$  being normal to the surface. Trajectories with different combinations of  $\alpha$  and  $\theta$  are integrated backward in time for 200 days and color coded gray to indicate a lunar origin in this time period, blue to indicate an Earth origin, and white to indicate no intersections with the primaries. The structure observed in these points is examined in the following plots by comparison with the invariant manifolds of planar Lyapunov orbits to determine whether

the invariant manifolds may act as a guide for mission design to understand the behavior of these impactor trajectories. Two sample Lyapunov orbits found in Anderson and Parker<sup>17</sup> are replotted here in Figure 2. The Jacobi constants for these orbits were chosen so that the invariant manifolds of the Lyapunov orbits just graze the surface of the Moon. The Jacobi constants where the Lyapunov orbits cover the surface of the Moon were computed by Baoyin and McInnes<sup>13</sup> as approximately  $C = 3.12185282430647$  for an  $L_1$  Lyapunov orbit and  $C = 3.09762627497867$  for an  $L_2$  Lyapunov orbit. Kirchbach et al.<sup>14</sup> compared the invariant manifolds of

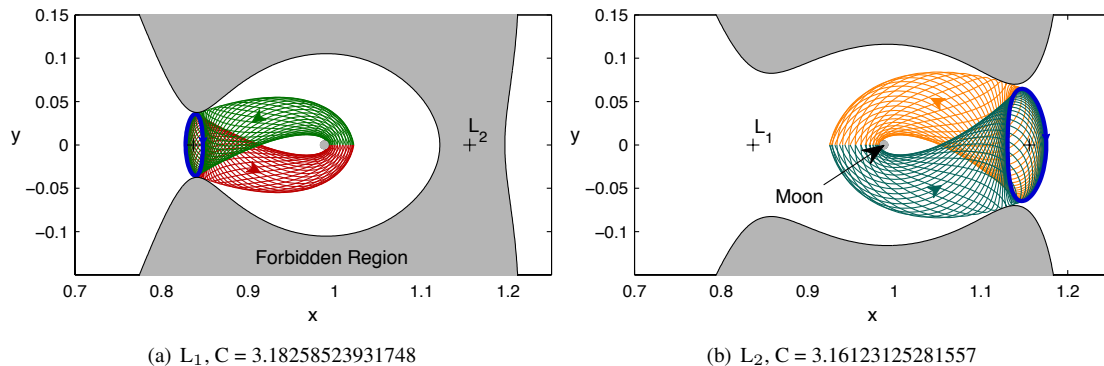


**Figure 2. Manifolds of libration orbits computed for Jacobi constants where the manifolds are tangent to the surface of the Moon.**

an  $L_1$  Lyapunov orbit using this technique for the escape case in the Jupiter-Europa system for a single value of Jacobi constant. They confirmed for this case that the invariant manifolds act as a boundary between the escape and non-escape cases as expected from Conley's theory. It is natural to question whether the invariant manifolds also act as boundaries between those trajectories originating from different bodies or elsewhere, and this question is explored here. Specifically, the same technique is used to examine impact trajectories using the invariant manifolds of both the  $L_1$  and  $L_2$  Lyapunov orbits in the Earth-Moon system over a wide range of Jacobi constants. The insights gleaned from this planar analysis are then used to aid in understanding the more complicated spatial problem.

In order to obtain an overview of the variation of the invariant manifold's intersections with the surface of the Moon, the Lyapunov orbits and their corresponding unstable manifolds were computed for a larger range of Jacobi constants in the CRTBP. A selected subset of the plots for several Jacobi constants are shown in Figure 3. One of the initial questions to be answered in computing the invariant manifolds is related to how long the integration duration should be. For mission design purposes, the approach from the Lyapunov orbit should typically be less than the duration of 200 days allowed for transfers from the Earth to the Moon. However, sufficient time should be allowed for the invariant manifolds to intersect the surface of the Moon and result in useful structure. A series of analyses were used with different integration times ranging from 50 to 200 days, and plots with sufficient structure were chosen for each Jacobi constant. The selected time duration for the integration of the invariant manifolds is noted for each plot with the most common duration being 25 dimensionless time units or approximately 109 days. Note that the longer integration times often showed more of the points of the invariant manifolds around additional structures not necessary for the current analysis, but filling these points in densely would require significantly more computational effort. In each case, the background points indicating the origin of the trajectory were all integrated for 200 days.

Examining the results in Figure 3, it is apparent that the manifolds are influential in dividing types of motion of the trajectory into different categories. The trajectories coming in to impact the lunar surface from other regions at  $C_{L_2}$  and  $C_{Avg(L_1, L_2)}$  are bounded by the invariant manifolds of the  $L_1$  Lyapunov orbit. This is similar to the results seen in Kirchbach et al. When both the  $L_1$  and  $L_2$  Lyapunov orbit invariant manifolds are shown for lower Jacobi constants, it is apparent again that they play a significant role in dividing the regimes of motion. In several cases, the invariant manifolds of the  $L_1$  orbit bound one side of the lunar origin trajectories, and the invariant manifolds of the  $L_2$  orbit bound the other side of these trajectories in the plot.

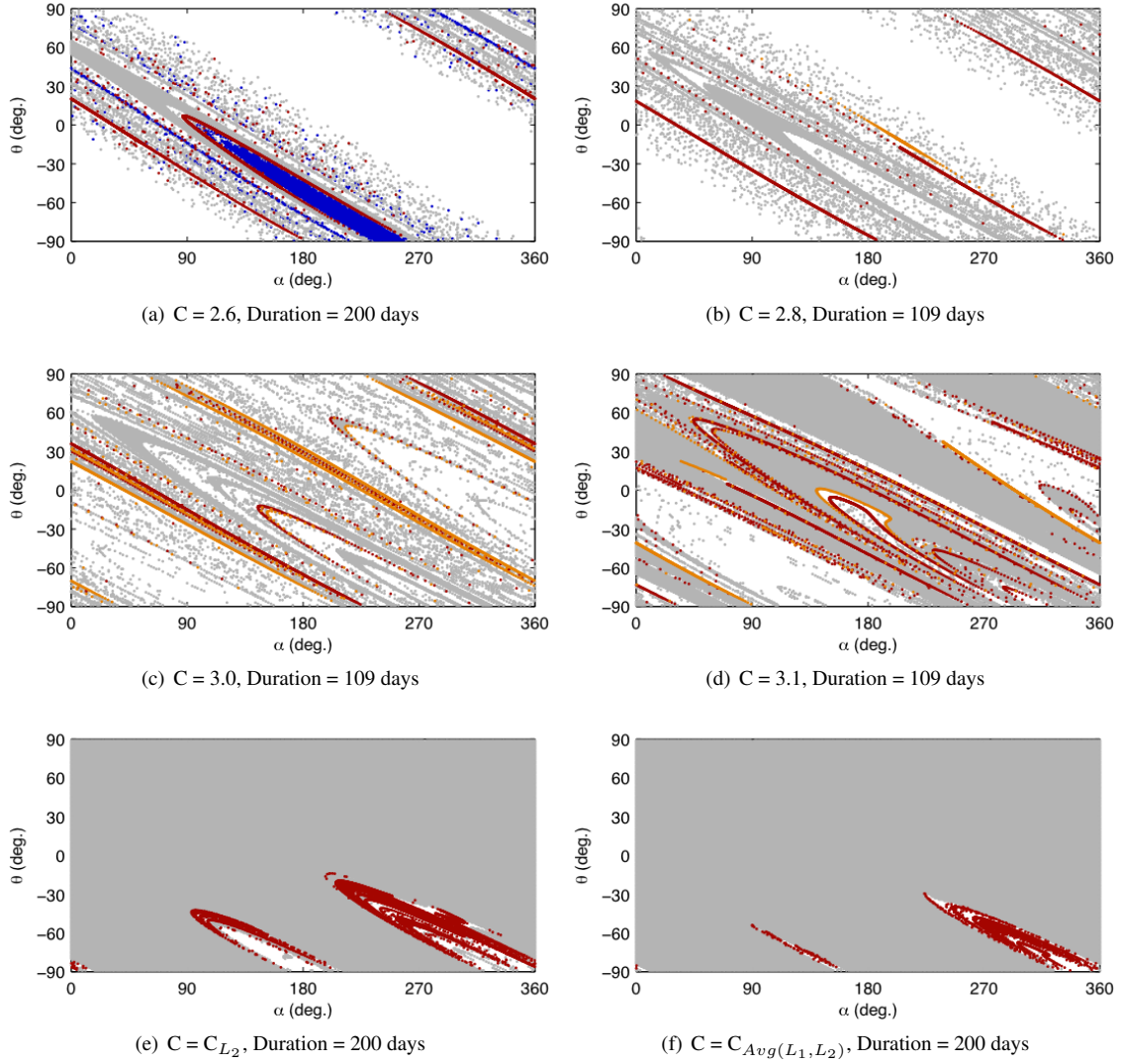


**Figure 3. Comparison of the origin of the trajectories at each  $\alpha, \theta$  point to the invariant manifolds of the  $L_1$  and  $L_2$  Lyapunov orbits. Gray indicates the trajectory originated at the Moon and blue that it originated at the Earth. Red points are the intersection of the  $L_1$  unstable manifold with the Moon, and orange corresponds to the  $L_2$  unstable manifold.**

For the  $C = 2.6$  case, the invariant manifolds of the  $L_1$  orbit segregate the most predominate set of Earth-origin trajectories from the rest. It is apparent from this result that the invariant manifolds play a significant role in transfers between bodies. More specifically, the invariant manifolds form a boundary between the trajectories originating at the Earth and those originating at the Moon. It should be noted that these invariant manifold points only show up when the integration time is increased to approximately 200 days. It is also interesting that although the manifolds form boundaries in the plots, they do not always strictly separate the points coming from different origins. This has to do in part with the length of time that the trajectories and manifolds are integrated and the particular region of interest. One of the reasons for this will be discussed next.

Some of the characteristics of these boundaries and the way in which trajectories follow the invariant manifolds in position space may be further explored by examining some cases involving specific trajectories

in more detail. One interesting case occurs for  $C = 3.1$  in Figure 3(d) where the trajectories transition from lunar origin trajectories to trajectories with no origin over the 200 day time span while crossing the line formed by the  $L_2$  Lyapunov orbit unstable manifold. They then transition back while crossing the  $L_2$  manifold again. A particular case may be taken by moving across  $\alpha$  from  $130^\circ$  to  $180^\circ$  while holding  $\theta = -3^\circ$ . Selected trajectories computed along this line are shown in Figure 4. For this case, the selected  $L_2$  manifold trajectories bound most of the trajectories originating elsewhere (shown here as black), while the lunar-origin trajectories lie on either side of the manifolds at the initiation of the backward integration. The invariant manifold trajectories act as a boundary between the trajectory types as they circle around the Earth twice in the rotating frame until the trajectories traveling backward in time approach the Moon once again. At

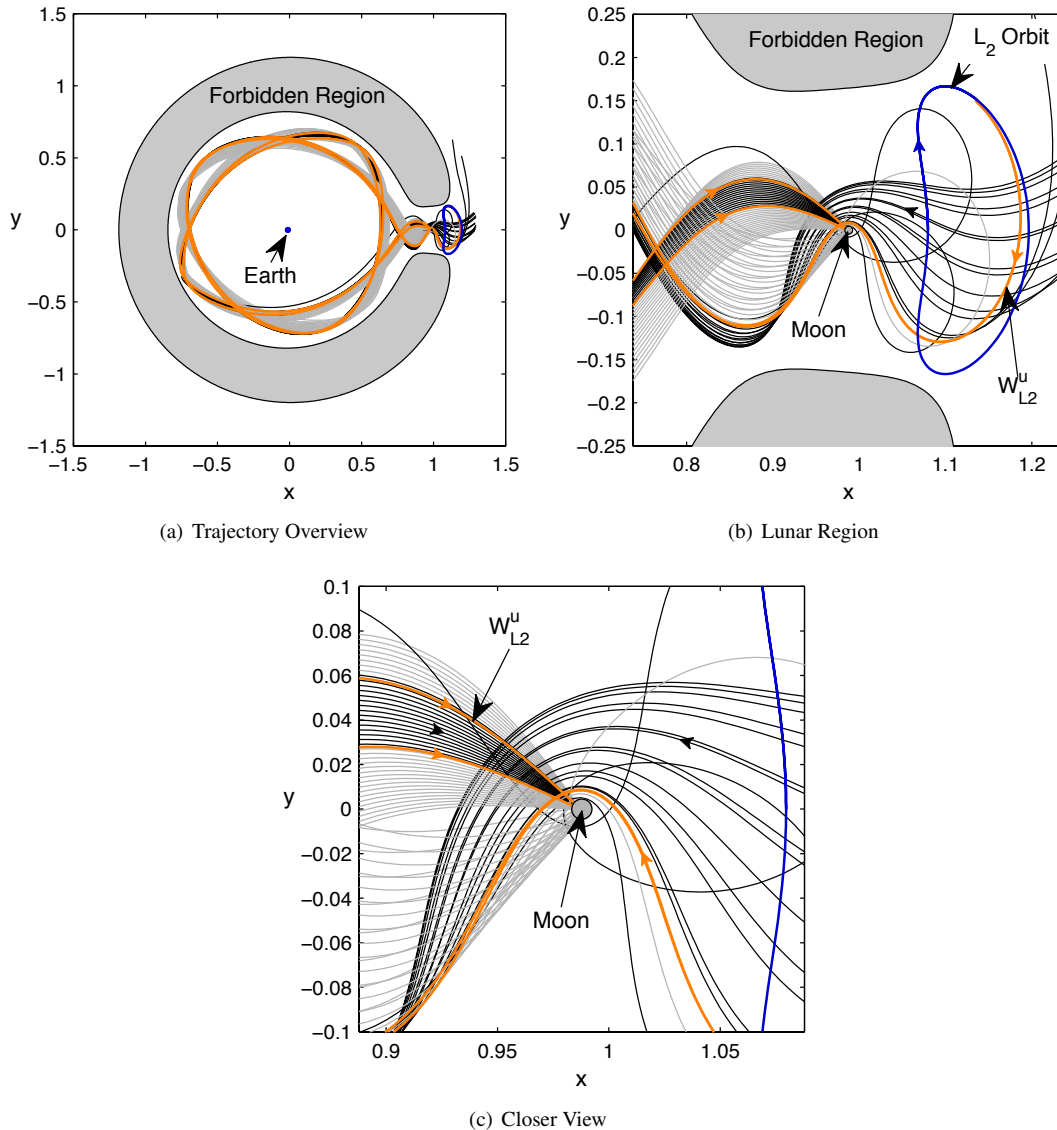


**Figure 4.** Comparison of selected trajectories plotted in position space for the  $C = 3.1$  case to unstable manifold trajectories of the  $L_2$  Lyapunov orbit. The trajectories are selected from the line at  $\theta = -3^\circ$  with  $130^\circ < \alpha < 180^\circ$ . The two trajectories on  $W_{L_2}^u$  are the ones intersecting nearest the selected line.

this point, the invariant manifolds approach the  $L_2$  Lyapunov orbit, the lunar-origin trajectories encounter the Moon, and the other trajectories generally travel through the  $L_2$  gateway and away from the Moon. One exception to this is a trajectory lying just outside of the guiding invariant manifold trajectories. Given its location it might be expected that it would be a lunar origin trajectory, however, it passes just above the surface of the Moon, spends some time in the neighborhood of the Moon, and returns to the interior region. This behavior is worth describing in more detail. The invariant manifolds are guiding the trajectories, and indeed only those trajectories starting between the manifolds could originate through the  $L_2$  gateway. The trajectory of interest was forced to remain in the vicinity of the Moon, but here, the important independent parameter of the Moon's radius comes into play. If the Moon possessed a larger radius, this trajectory would have originated at the Moon. If the Moon's radius were smaller, other trajectories would be observed that failed to originate at the Moon. This indicates that the invariant manifolds can guide the trajectories and keep them in a region where they are likely to impact a body, but impact may not always occur depending on the constraint of the body's radius. This behavior leads to some fuzziness in the boundaries observed in the previous plot. It can also be seen that if the trajectories are integrated long enough they are likely to return to encounter the Moon at an earlier time. Once these exterior trajectories return, other structures may be observed indicating that additional dynamical structures may be at play in the trajectories' behavior.

An additional case was selected to analyze the effects of two different manifolds on the trajectories, and the results are given in Figure 5. For this case, selected trajectories were taken from the bend indicated in the inset of Figure 5(a). Single trajectories from the invariant manifold of both the  $L_1$  and  $L_2$  Lyapunov orbits were taken from the bends in the curves. Trajectories selected from the lunar-origin trajectories and just outside this region were then integrated and plotted as shown in Figure 5. This case is more complicated than the previous case, but the guiding effect of the invariant manifolds may still be observed. For this case, the integration for the lunar impacting trajectories is started as shown in the inset of Figure 5(b), and as the integration progresses, the trajectories travel once around the Earth in the rotating frame. As the trajectories approach the Moon, the trajectories between the manifolds are found to originate at the Moon. Those on the other side of the  $L_1$  Lyapunov orbit travel through the  $L_1$  gateway into the interior region, and those

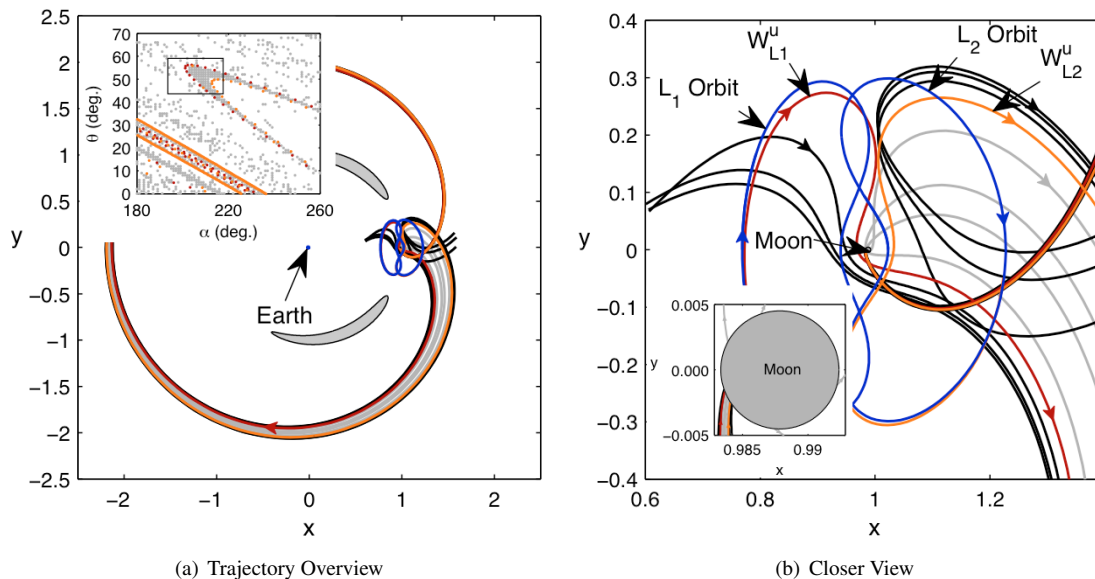


**Figure 5. Comparison of trajectories on the unstable manifolds of the  $L_1$  and  $L_2$  Lyapunov orbits to selected trajectories impacting the Moon for  $C = 3.0$ . The points used to compute the trajectories were taken from the box in the inset of (a). They included a trajectory from each manifold on the bend of the curve and points selected by hand between the manifolds (that originate at the Moon) and just outside the manifolds.**

on the other side of the  $L_2$  Lyapunov orbit travel through the  $L_2$  gateway to the exterior region. Again, the trajectories that originate at the Moon would be affected by the radius of the Moon, but the invariant manifolds generally guide the trajectories to where they have a greater chance of an encounter with the Moon.

In general the dynamics are more complicated and difficult to analyze in position space than in the lunar surface intersection plots. It is clear, however, from this two-dimensional analysis that the invariant manifolds are influential in guiding the Earth and Moon-origin trajectories from their respective origins. These results imply that similar mechanisms may be at work in the three-dimensional problem, and this topic is the focus of the remainder of this study.

### THREE-DIMENSIONAL ANALYSIS

The planar CRTBP provides a convenient framework in which to understand and visualize the relationship between invariant manifolds and lunar approach trajectories, but the design of real-world equivalent trajectories often requires a landing at either higher or lower latitudes. Indeed, many of the recently proposed landing sites at the Moon are at northern or southern latitudes,<sup>27</sup> and one of the locations that is currently a focus for a lunar lander is more southern latitudes in the Aitken Basin. In this analysis, lunar landing trajectories are analyzed over the three-dimensional surface of the Moon, and the approach geometry of the trajectories in three dimensions is analyzed. The approach trajectories following the invariant manifolds of various spatial libration point orbits are then compared to these lunar landing trajectories.

#### Earth-Moon Landing Geometry

The landing geometry of trajectories traveling from the Earth to the Moon is of particular importance for mission design. In our previous paper<sup>17</sup> we analyzed trajectories encountering the Moon normal to the surface to determine whether these trajectories originated at the Earth within the previous 200 days. Given this elevation angle constraint, only some locations of the Moon's surface were found to be accessible from the Earth. For this analysis, trajectories were allowed to approach each point on the lunar surface from all directions. These directions were specified relative to the surface at each point. The azimuth angle ( $\Omega$ ) is measured clockwise from north where north is the lunar orbit's north pole, rather than the Moon's north pole to be consistent with the results from the CRTBP. The elevation angle ( $\phi$ ) is measured positive above the Moon's surface with a trajectory encountering the Moon's surface normal to the surface having an elevation angle of  $90^\circ$ . (Note that this is different from  $\theta$  used for the planar case, but it was chosen to be more consistent with typical mission design parameters.) While the previous analysis was ideal for impactors, the trajectories computed here are applicable for a wide range of mission types traveling to the lunar surface. Additional parameters for each trajectory related to the original characteristics relative to the Earth may be computed as in our previous paper, but the focus here is on characterizing the approach geometry. For the following analysis the trajectories were computed over the surface of the Moon using  $1^\circ$  increments in  $\alpha$  and  $\beta$ . The same definition is used for  $\alpha$  that is used in the planar problem in Figure 1.  $\beta$  is measured like latitude and is positive above the  $xy$  plane. Two different grids were used for the azimuth and elevation angles. In each case, the elevation angle was varied in even increments, and the steps taken in azimuth angle were specified initially for an elevation angle of  $0^\circ$ . The number of azimuth points were then decreased with  $\cos(\phi)$  so that the number of points decreased with elevation angle. Both a fine grid and a coarser grid were used in this analysis. For the fine grid case,  $1^\circ$  increments were taken at  $0^\circ$  elevation for  $\Omega$ , and  $1^\circ$  increments were used for elevation. For the coarser grid,  $10^\circ$  increments were used for  $\Omega$  at  $0^\circ$  elevation, and  $3^\circ$  increments were used for elevation. This coarser grid was found to provide a good approximation that conveyed the overall trends of the fine grid, while allowing for a more reasonable computation time. Even with this coarser grid, computing trajectories over the entire surface in the ephemeris problem for each Jacobi constant required approximately seven days running in parallel on 40 processors. Unless otherwise stated, this coarser grid is the one used throughout the analysis.

As an initial step in the analysis, the set of trajectories were computed in the CRTBP for a Jacobi constant of 2.6. The trajectories were computed for both the fine grid and the coarser grid. A comparison of the maximum and minimum elevation angles resulting in trajectories that originate at the Earth is shown in Figure 6. Using the symmetry about the  $xy$  plane mentioned earlier, it can be seen that the northern and southern latitudes

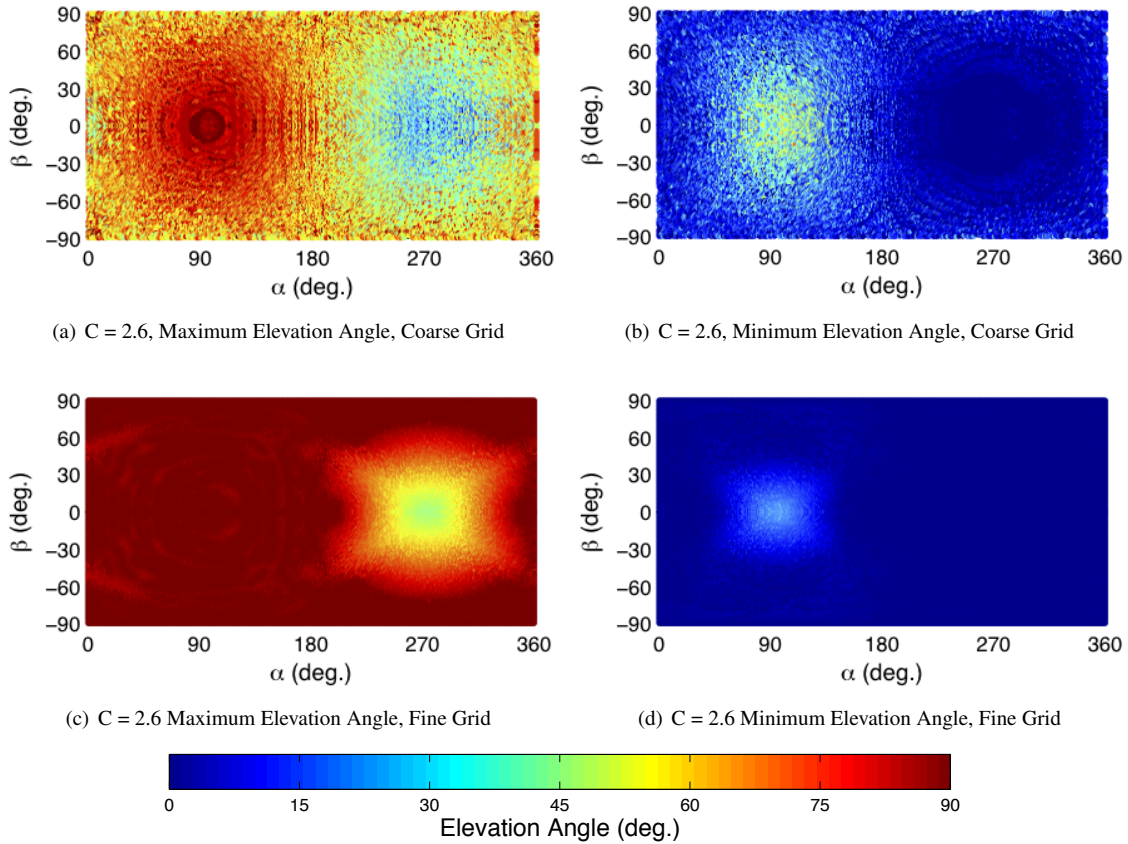


**Figure 6. Maximum and minimum elevation angles for trajectories originating at the Earth and encountering the Moon at each point on the surface. These cases are computed in the CRTBP for  $C = 2.6$ . Results from two different grids (in elevation and azimuth angle) are shown.**

will be reflected for the elevation plots in the CRTBP. Note that the azimuth angles would need to account for the reflection if they are plotted, and although similar results would be expected in the ephemeris problem, the variations in the ephemeris require that the northern and southern quadrants be computed independently. Using this symmetry the values computed for the northern and southern hemispheres were reflected in Figure 6 to save computation time. By comparing the plots, it can be seen that, as might be expected, the finer grid captures more trajectories at higher and lower elevation angles that originate at the Earth, however, the overall trends in the data remain the same for both grids. In each case the range of elevation angles from minimum to maximum is higher near  $\alpha = 90^\circ$  and lower near  $\alpha = 270^\circ$ . Referring back to Figure 1, the  $90^\circ$  direction corresponds to the leading edge of the Moon, and the  $270^\circ$  direction to the trailing edge. The coarser grid is used in the remainder of this analysis, so it should be remembered that details in the plots may change with a finer grid, but the overall trends can still be observed.

An analysis of trajectories for a Jacobi constant of  $C = 2.8$  confirmed our earlier result for trajectories encountering the Moon normal to the surface of the Moon that no Earth return trajectories were found for this Jacobi constant or higher ones in the CRTBP. However, it is expected that Earth-origin trajectories with velocities consistent with higher Jacobi constants in the CRTBP will exist in the ephemeris problem because these trajectories may use the Sun's perturbations to travel from the Earth to the Moon. Those higher Jacobi constants, especially those approaching the values near  $C_{L_1}$  and  $C_{L_2}$  are especially relevant for the computation of the invariant manifolds of libration point orbits which is useful for the comparison later in this study. The elevation angle range results are shown in Figure 7 for Jacobi constants ranging from  $C = 2.6$  to 3.1 in

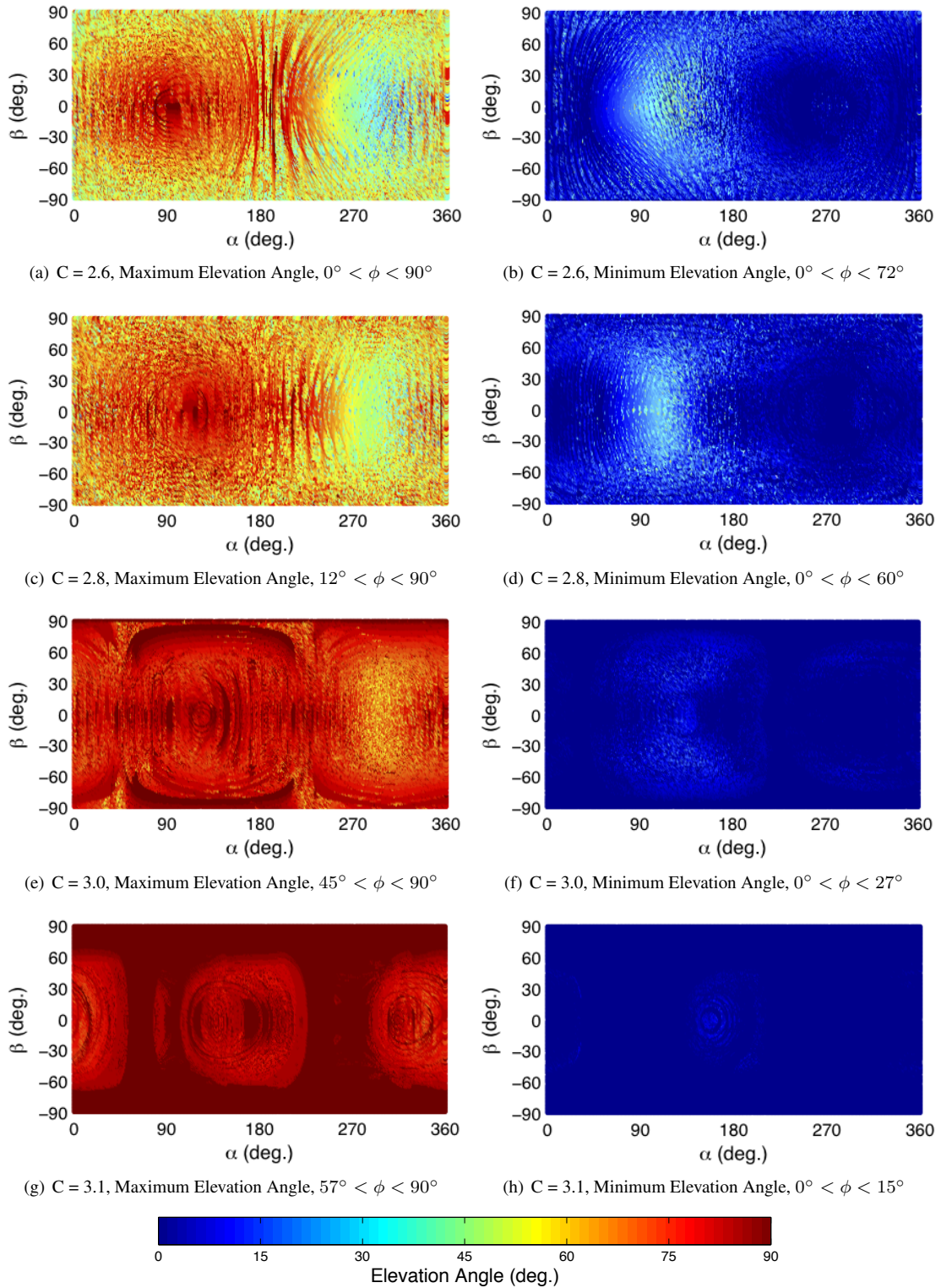


**Figure 7. The minimum and maximum elevation angles of trajectories originating at the Earth for each point on the lunar surface. These trajectories are computed in the Earth-Moon ephemeris system including the Sun's perturbations.**

the ephemeris problem. Note that, as in our previous paper,<sup>17</sup> the Jacobi constant for the ephemeris plots is used as a shorthand for a particular set of velocities computed around the Moon in the CRTBP. These same velocities are attached to the Moon in the ephemeris problem referenced to the instantaneous orbital plane of the Moon's orbit around the Earth. The symmetry used to simplify the computations in the CRTBP is no longer present for the ephemeris problem, and trajectories were directly computed for the entire plot. Once the trajectory is integrated backward from the Moon, the Jacobi constant of the trajectory will vary in both the Earth-Moon and Sun-Earth systems.

Comparing the results from Figure 6 for the Jacobi constant case of 2.6 in the CRTBP and the ephemeris problem results reveals that they are quite similar. The maximum and minimum elevation values still occur at approximately the same locations on the surface for each case. However, several new bands of high elevation angle cases occur for the ephemeris case near  $\alpha = 180^\circ$  for the maximum elevation angle case and from approximately  $\alpha = 290^\circ$  to  $360^\circ$ . Additional bands also seem to exist for the minimum elevation angle case, especially for high and low latitudes. It is natural to expect from past work that these bands may represent trajectory options that exist as a result of the Sun's influence, and it is interesting that these types of bands remain up through  $C = 2.8$ . An interesting topic planned for future study is to determine how these characteristics vary with a finer grid. However, the comparison performed here is with the same grid in each case, indicating that these additional trajectories exist.

As the Jacobi constant increases even more as seen in Figures 7(e) through 7(h), the range of elevation angles for lunar landing at each point seems to increase even more. The location of the peaks also seems to shift, and for the maximum elevation angle plots, the peaks move to the right or eastward with increasing Jacobi constant. When a Jacobi constant of 3.1 is reached, the maximum elevation angle for points containing a trajectory originating at the Earth never drops below  $57^\circ$ , and the minimum elevation angle for the same points never goes over  $15^\circ$ . It is important to mention that although the points look dense across the surface in the plots, this is because of the size of the plot and the points used for plotting. There are individual points on the surface where no Earth-origin trajectory exists for this grid, but there are always nearby points where such a trajectory exists. For real-world mission design, a small  $\Delta V$  can be used to target slightly different points, and the surface of the Moon is practically covered for mission design purposes. It has also been found for particular points that if a much finer grid is used, typically some Earth-origin trajectories are found, and these points will be included in future studies. The points with no Earth-origin trajectories for this grid are not included in the elevation angle ranges listed in the plots. These results for higher Jacobi constants agree generally with the normal trajectory cases seen in our previous work. The additional range of geometries available for landing at these energies appears to be a result of the increasingly chaotic nature of the system as the Jacobi constant approaches the values at the  $L_1$  and  $L_2$  libration points. In other words, the trajectories are more able to take advantage of chaos to arrive at different elevation and azimuth angles. This also indicates that these Jacobi constants are of particular interest for comparison with the invariant manifolds of libration orbits. One interesting statistic to examine is the maximum number of trajectories at a particular point that originate at the Earth. Although this number is generally quite low, there are some points where it peaks. The maximum number of trajectories at a particular point is listed in Table 2 for different Jacobi constants. The higher values are found for a Jacobi constant of 2.6 and 3.1. The  $C = 2.6$  results include more direct trajectories that still exist in the CRTBP and do not require the Sun's influence, and the  $C = 3.1$  results include those trajectories that are heavily influenced by the Sun. The total number of Earth-origin trajectories follows the same trend. These numbers are a function of the grid that is being used and can be refined by using a denser grid, however they do align with the results from the trajectories computed normal to the lunar surface seen in our earlier work.

Because the trajectories are computed in the ephemeris problem for the cases just discussed, the results will naturally vary with the initial epoch of the integration. A sample of the results was computed for four different epochs around the Moon's orbit at seven day increments (approximately one-quarter of the Moon's orbit) to determine how they might vary with the initial epoch. Representative results for a Jacobi constant of 2.8 are shown in Figure 8. The salient features of the plots remain generally the same for each epoch in that the maximum values still occur near  $\alpha = 90^\circ$  and the minimum values occur near  $\alpha = 270^\circ$ . The January 7 and 21 cases have more locations with higher elevation angles, especially near  $\alpha = 270^\circ$ , mixed

**Table 2. Maximum number of Earth-origin trajectories at a single point on the lunar surface including the corresponding location and the total number of Earth-origin trajectories for various values of Jacobi constant.**

Jacobi Constant	Maximum at a Point	Location ( $\alpha, \beta$ )	Total Number
2.6	27	(193°, -36°)	290,672
2.8	16	(213°, -18°)	114,684
3.0	14	(225°, -11°)	162,061
3.1	36	(192°, 7°)	298,621

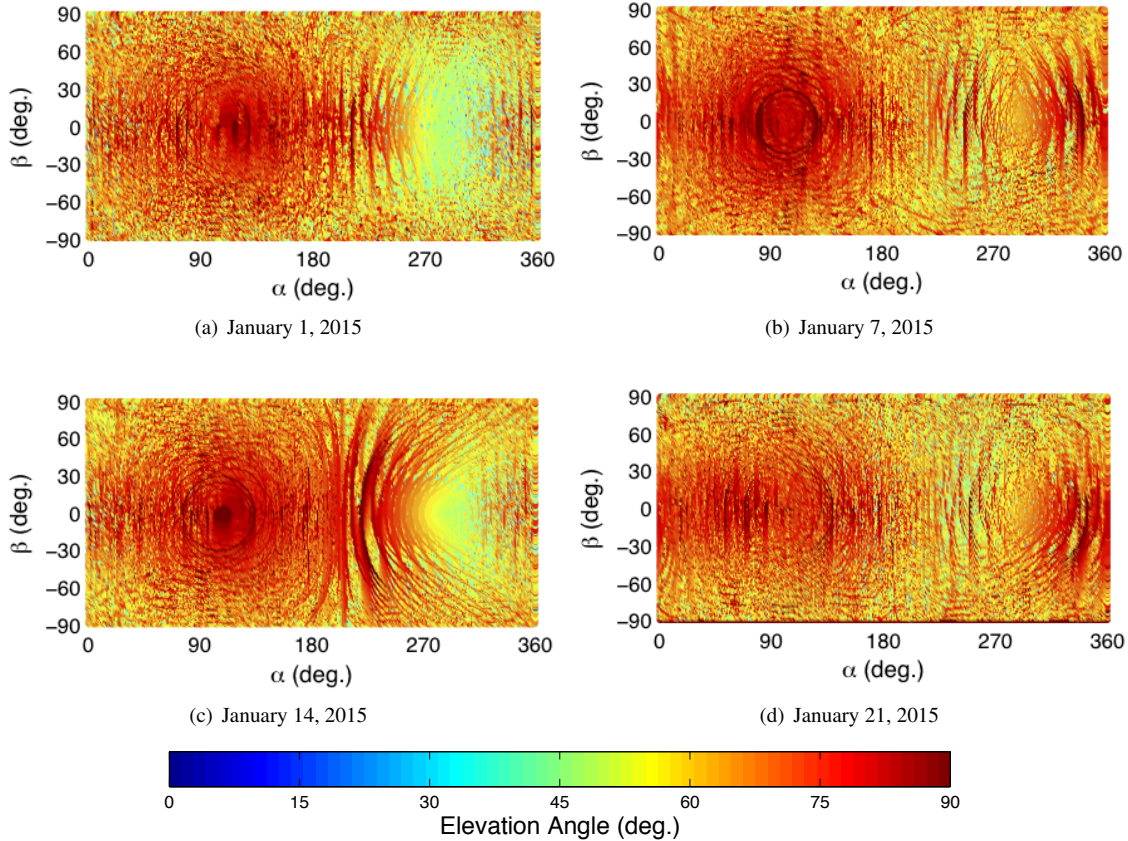


**Figure 8. Comparison of maximum elevation angle results around the lunar orbit at seven day intervals for  $C = 2.8$ .**

in with lower elevation angle points. These two cases appear better positioned to take advantage of the Sun-Earth libration point dynamics, which could increase the range of elevation angles that may be obtained for approaching the Moon. Overall though, given this comparison, it is expected that the results from this study may be extrapolated to other epochs without drastically changing the outcome.

Another important aspect of the approach for mission design is, of course, the azimuth angle of the trajectory. Plotting this information in a global sense is difficult, but a sample of the types of results obtained for each Jacobi constant may be visualized for a subset of the points in Figure 9. The azimuth angles are plotted for each point on a grid computed at  $30^\circ$  intervals in both  $\alpha$  and  $\beta$ . For these plots, the fine grid was used at each point on the surface which of course produced more trajectory options. The orientation of the

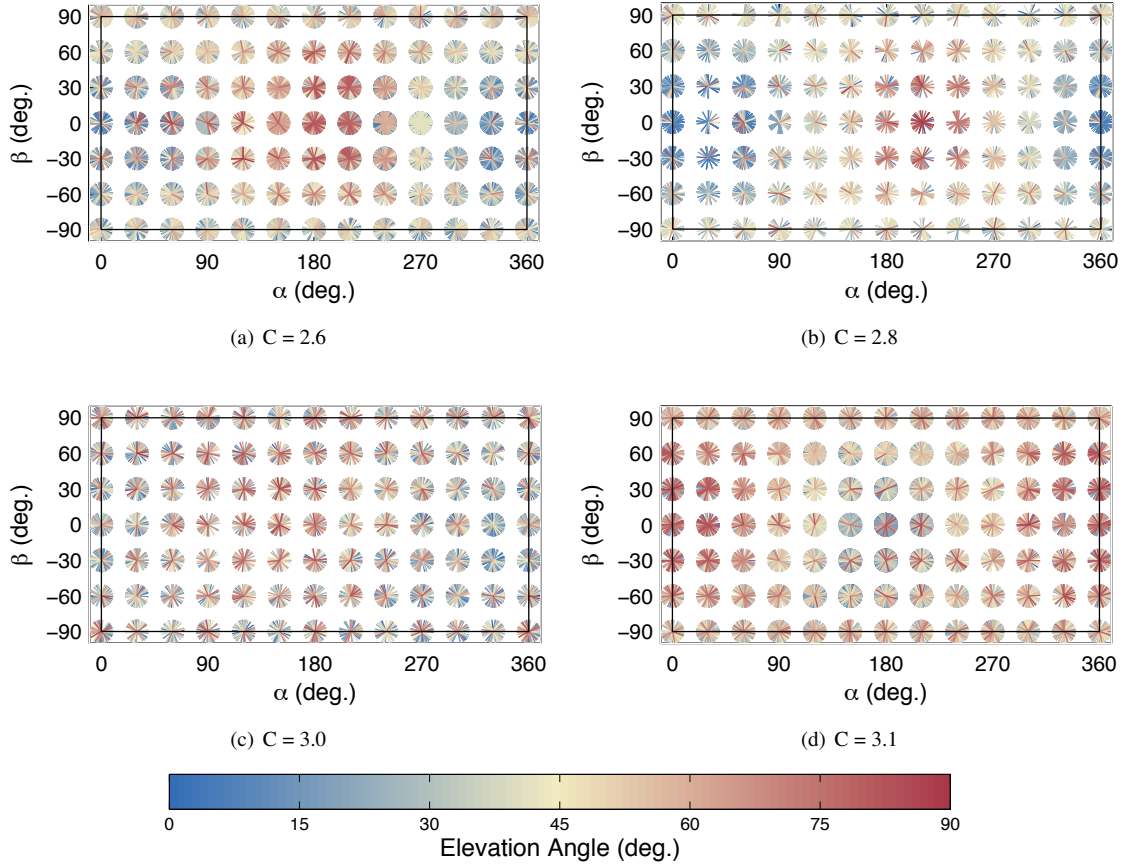


**Figure 9. Azimuth angles at points on a  $30^\circ$  grid on the lunar surface. The plotted lines at each gridpoint are oriented in the proper azimuth direction for each individual trajectory. The color corresponds to the elevation angle of that trajectory.**

lines centered on each point indicates the azimuth angle, and the color is used to designate the corresponding elevation angle of each trajectory. Note that the  $\pm 90^\circ$  cases used azimuths that were rotated differently at each elevation as a result of the transformation used to compute them. So the specific results differ, but they generally show similar trends. It is interesting that there are definite regions where the majority of Earth-origin trajectories appear to have similar elevation angles. In each case though, there are often just a few high or low trajectories that result in the extremes seen in the elevation angles plots. This fact is worth keeping in mind for mission design since a particular elevation angle may only be available in combination with only a few azimuth angles. In general it appears that higher elevation options are more available as the Jacobi constant increases, although there are typically at least a few low elevation angle options at each point. The combinations of available elevation and azimuth angles are evaluated more directly for  $C = 3.1$  in the comparison with invariant manifolds, which will help explain the features seen in these plots a little more directly. Nevertheless, these plots can provide a broad overview of the available trajectory options.

### Invariant Manifold Analysis

The invariant manifolds of libration orbits in the planar problem were found to provide general boundaries to different regimes of motion in the planar CRTBP. It is expected that similar types of behavior exist in phase space for the three-dimensional problem. However, with the increase in the dimension of the problem, the visualization of the invariant manifolds compared to the Earth-Moon landing trajectories becomes drastically

more difficult. Spatial comparisons are therefore made using the intersection geometry of the invariant manifolds of libration orbits with the Moon and by looking in detail at specific landing locations on the Moon. For this comparison, halo orbits computed within the CRTBP are used, and a rough comparison with the ephemeris results is performed. This technique ensures that the velocities at specific points on the Moon are the same for each case. It has also been found that over the short integration times used for the invariant manifolds to travel from the halo orbit to the Moon, the Sun should have little time to perturb the trajectory, and it should remain similar to those computed in the ephemeris problem. The transfers to the halo orbits from the Earth are not analyzed here because techniques for performing these transfers using the Sun's influence are summarized in Parker's dissertation.<sup>12</sup> More detailed analysis in the ephemeris problem will be performed in the future.

As a first step in the comparison, the lunar landing geometry of the invariant manifolds of various halo orbits is analyzed. Alessi, Gómez, and Masdemont<sup>15</sup> examined similar trajectories for escaping the surface of the Moon to various halo orbits and summarized the areas on the Moon from which such escape trajectories are possible. We are concerned here with a combination of the landing location along with the landing geometry, therefore, a similar technique as that used in Figure 9 is employed here. The intersections of the unstable manifolds of the  $L_1$  halo orbits are indicated by a red point, and the intersections for the  $L_2$  halo orbits are orange points. The azimuth angle and the elevation angle are indicated by the direction and the color, respectively.

The results for a halo orbit at  $C = 3.1$  are shown in Figure 10. It can be immediately seen that for this energy, the  $L_1$  halo orbit manifolds generally fall on the leading edge of the Moon in its orbit, and the  $L_2$  halo orbit manifolds fall on the trailing edge of the Moon. As expected, the intersections of the northern and southern halo orbits are reflected about  $\beta = 0$ . The elevation angles are somewhat lower for the  $L_1$  halo orbits than the  $L_2$  halo orbits. All together, the unstable manifolds provide relatively broad coverage of much of the lunar surface, although still significant regions are not intersected by the manifolds. This may be potentially remedied by examining the manifolds at additional energies. The unstable manifold intersections with the Moon can change significantly with the Jacobi constant as can be seen for the intersections plotted with a Jacobi constant of 3.08 in Figure 11. The intersections for the  $L_1$  case have divided into two different regions, and the  $L_2$  intersection case has grown tighter together. It should be reiterated that the unstable manifold intersections can increase if larger time intervals are used for the integration, and these plots focus on short-duration trajectories. The unstable manifold intersections also change even more as energy continues to change, but these energies appear to provide some of the most direct transfers.

This analysis shows that the unstable manifolds of halo orbits can provide broad coverage for landing at various points on the Moon, although not with the nearly complete coverage found from the previous results. It is also interesting to explore the relationship between the unstable manifolds and these Earth-origin trajectories from the general analysis. A similar examination to the one made for the planar problem would be desired, but the nature of the three-dimensional problem makes this drastically more complex. One possible method for performing this comparison is to examine the origin of the trajectories coming from all azimuth and elevation angles at each point that the unstable manifolds intersect the surface of the Moon. In this case, only one unstable manifold intersection is plotted for each point relative to the trajectories coming in from all angles, but it still allows this point to be placed in context of the dynamics indicated by the source of each trajectory.

An initial comparison with this technique was made in Figure 12 using points from the  $L_2$  northern halo orbit at  $C = 3.1$  since the unstable manifold intersections move across a broad portion of the Moon, and we are interested in trajectories that may travel through the  $L_2$  gateway to be influenced by the Sun. The results are plotted with each plot corresponding to one of the unstable manifold intersections with Moon. For these plots a fine grid stepping in one degree increments in both azimuth and elevation angle was used. Although the unstable manifold points are computed in the CRTBP, and the remaining points are computed in the ephemeris, the results are intriguing. The unstable manifold points in each case often lie on the boundary of the Earth-origin and lunar-origin trajectories. The primary set of Earth-origin trajectories appear to form a line or circle as the position is moved across the surface of the Moon, and comparing these results to Figure 9(d) sheds some light on why elevation angles are grouped together in that plot. In all cases, the unstable manifold

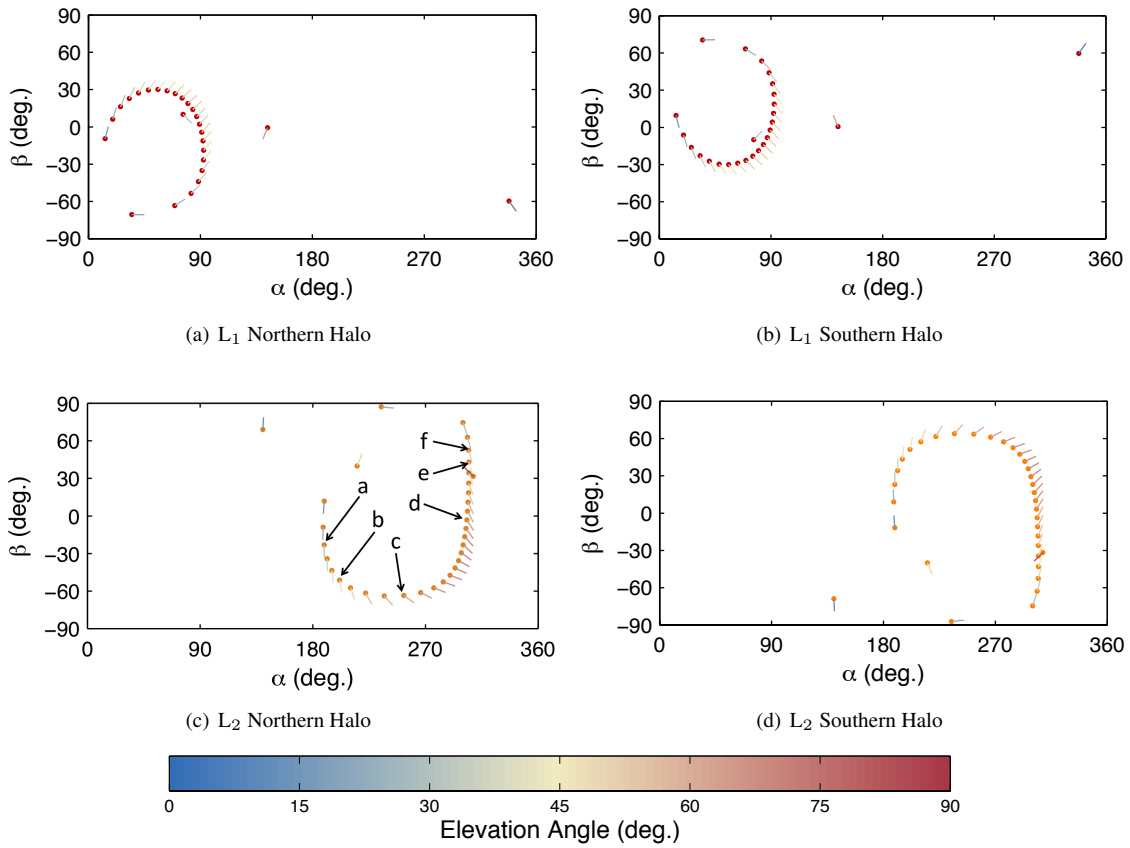


**Figure 10. Unstable manifold intersections of the specified orbits with the Moon for  $C = 3.1$ . The labels in (c) are used to designate the plots in Figure 12.**

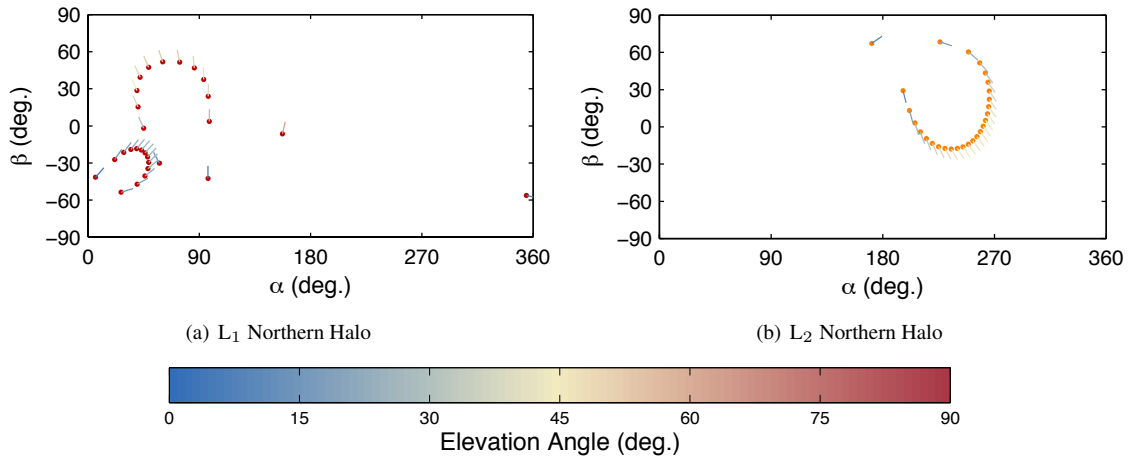


**Figure 11. Unstable manifold intersections of the specified orbits with the Moon for  $C = 3.08$ .**

point lies between this main set of Earth-origin trajectories and the larger band of lunar-origin trajectories. Although there is no line of unstable manifold points to separate the regimes of motion as in the planar

problem, the unstable manifold still appears to lie on the general boundary between the two trajectory types. The fact that such a relationship exists in the dynamics is an argument that the CRTBP unstable manifolds are a good approximation over short times to the unstable manifolds found in the ephemeris, but more work is needed to verify this statement.

Finally, it is interesting to examine several trajectories plotted in position space corresponding to the lunar surface intersections. Several trajectories selected from either side of the unstable manifold intersection in Figure 12(b) are plotted in Figure 13. Here it can be seen that the Earth-origin trajectories do indeed travel through the  $L_2$  gateway during the transfer while the lunar-origin trajectories do not. Remember that the  $L_2$  manifold is computed in the CRTBP, but it provides a guideline as to how the manifolds would behave in the ephemeris problem. If the Earth-origin trajectories are followed further to their source, it can be seen that they approach the  $L_1$  point of the Sun-Earth system and then either encounter the Earth directly or use phasing orbits to do so. It appears that this set of trajectories is following the invariant manifold pathways connecting the Sun-Earth and Earth-Moon libration orbit invariant manifolds found in Koon, Lo, Marsden and Ross,<sup>11</sup> Parker and Lo,<sup>8</sup> and Parker.<sup>12</sup> It also appears that the main band of Earth-origin trajectories follows this route, and that similar pathways may be targeted from each selected point on the Moon.

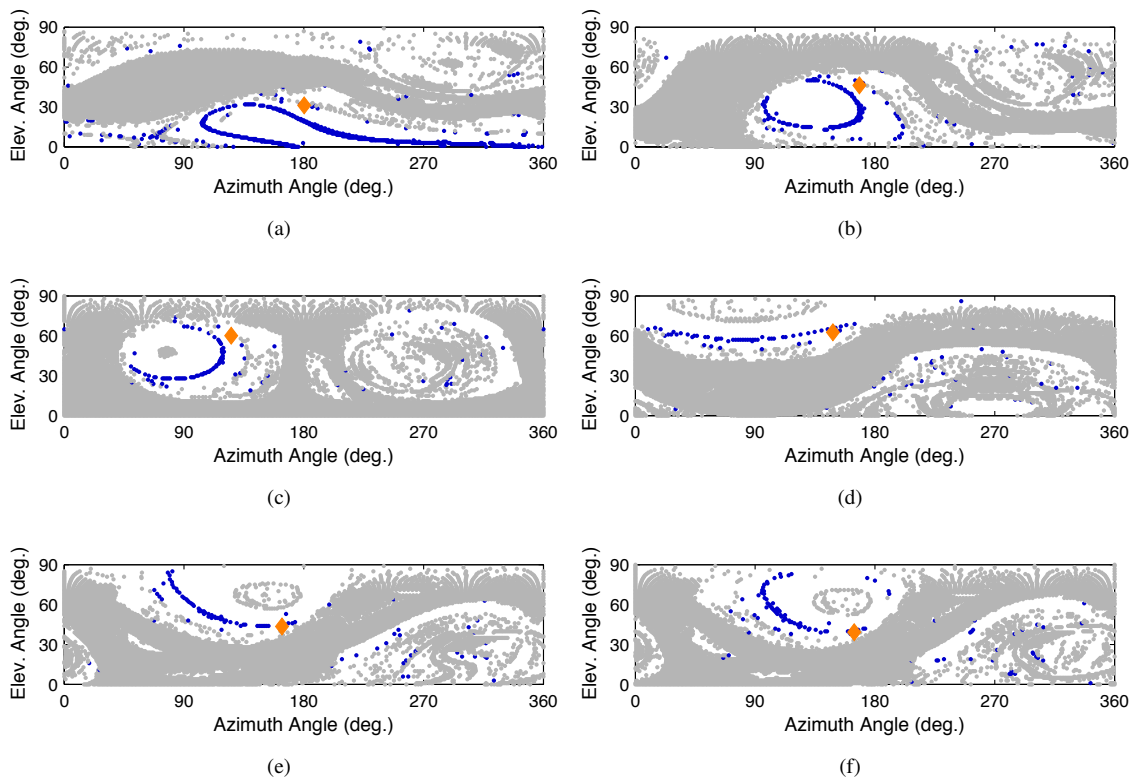


**Figure 12. The origin of trajectories plotted for various azimuth and elevation angles computed for several intersection points of the  $L_2$  northern halo unstable manifolds (indicated by the orange diamond) with the lunar surface. Each subfigure corresponds to the associated point as labeled in Figure 10(c). ( $C = 3.1$ )**

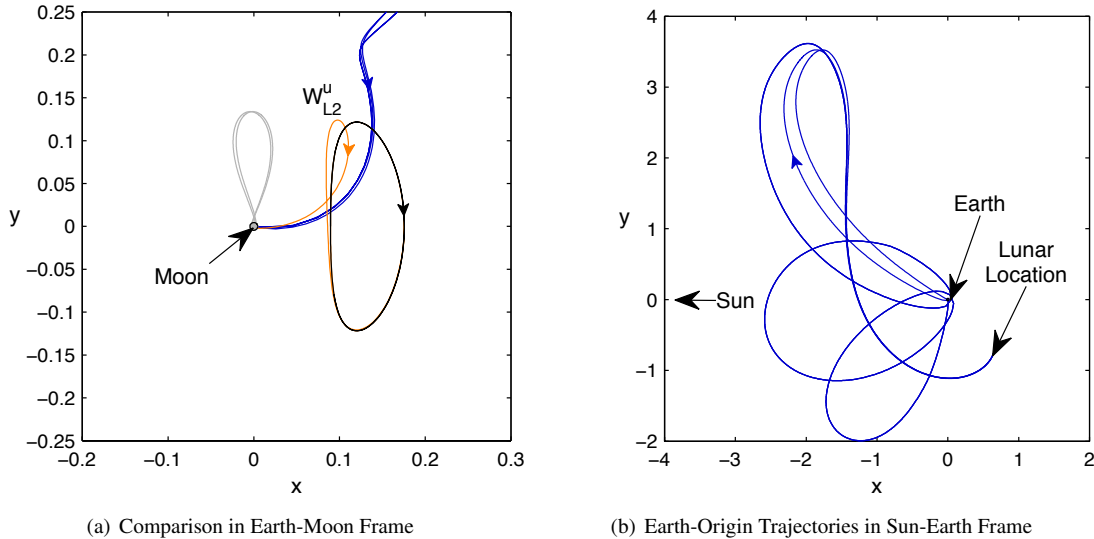


**Figure 13. Comparison of the selected Earth-origin, lunar-origin and invariant manifold trajectories in the Earth-Moon and Sun-Earth rotating frames. The  $L_2$  unstable manifold trajectory is superimposed on the plot because it is computed in the CRTBP.**

## CONCLUSIONS

The characteristics of Earth and lunar-origin trajectories encountering the lunar surface at different elevation angles have been quantified and compared to the invariant manifolds of libration orbits in both the planar and three-dimensional problem. In the planar problem, the unstable manifolds of Lyapunov orbits were shown to generally bound the different regimes of motion between the trajectories with different origins. The boundaries were explored, and it was shown that some points may cross the boundary as a result of factors such as the radius of the Moon and the chosen integration time. A wide range of elevation angles were shown to be available for landing at different points on the Moon for different Jacobi constants in the three-dimensional problem with higher elevation angles generally available on the leading edge of the Moon and lower elevation angles possible on the trailing edge. The invariant manifolds of halo orbits were shown to provide coverage of a large portion of the Moon's surface with small changes in Jacobi constant allowing a wider coverage. The particular approach of the unstable manifolds of the  $L_2$  northern halo orbit was found to lie generally on the boundary between the set of Earth-origin trajectories and a band of lunar-origin trajectories. The Earth-origin trajectories from a particular sample appear to transit through the  $L_2$  gateway and travel near the Sun-Earth  $L_2$  libration point on their journey from the Earth.

## FUTURE WORK

The results from this study bring up many possible avenues for future work. A more refined grid in the ephemeris problem will likely allow a more detailed analysis of the possible connections between the Earth and the Moon. Different integration times for the different trajectories can be explored in addition to examining different epochs for the initial epoch in the integration. The halo orbits generated in the CRTBP for the comparison can also be generated in the ephemeris problem for a more detailed comparison. Finally, additional mission design parameters can be generated to aid in selecting particular trajectories for specific missions, and Earth departure characteristics can be generated.

## ACKNOWLEDGEMENTS

The authors would like to thank Ted Sweetser for his support and for making this work possible. They would also like to thank Roby Wilson and Damon Landau for their helpful comments and reviews of this work.

The research presented in this paper has been carried out at the Jet Propulsion Laboratory, California Institute of Technology, under a contract with the National Aeronautics and Space Administration.

## REFERENCES

- [1] Mission Evaluation Team, "Apollo 11 Mission Report," Tech. Rep. NASA SP-238, National Aeronautics and Space Administration, 1971.
- [2] S. B. Broschart, M.-K. J. Chung, S. J. Hatch, J. H. Ma, T. H. Sweetser, S. S. Weinstein-Weiss, and V. Angelopoulos, "Preliminary Trajectory Design for the ARTEMIS Lunar Mission," *Advances in the Astronautical Sciences, Astrodynamics* (A. V. Rao, T. A. Lovell, F. K. Chan, and L. A. Cangahuala, Eds.), Vol. 135, Part II, Pittsburgh, Pennsylvania, American Astronautical Society, Univelt Inc., 2009, pp. 1329–1344.
- [3] M. Woodard, D. Folta, and D. Woodfork, "ARTEMIS: The First Mission to Lunar Libration Orbits," *21st International Symposium on Space Flight Dynamics*, Toulouse, France, Centre National d'Études Spatiales, September 28 - October 2 2009.
- [4] R. B. Roncoli and K. K. Fujii, "Mission Design Overview for the Gravity Recovery and Interior Laboratory (GRAIL) Mission," *AIAA/AAS Astrodynamics Specialist Conference*, No. AIAA 2010-8383, Toronto, Ontario, Canada, August 2-5 2010.
- [5] M. J. Chung, S. J. Hatch, J. A. Kangas, S. M. Long, R. B. Roncoli, and T. H. Sweetser, "Trans-Lunar Cruise Trajectory Design of GRAIL (Gravity Recovery and Interior Laboratory) Mission," *AIAA Guidance, Navigation and Control Conference*, No. AIAA 2010-8384, Toronto, Ontario, Canada, August 2–5 2010.
- [6] S. J. Hatch, R. B. Roncoli, and T. H. Sweetser, "GRAIL Trajectory Design: Lunar Orbit Insertion through Science," *AIAA/AAS Astrodynamics Specialist Conference*, No. AIAA-2010-8385, Toronto, Ontario, Canada, August 2–5 2010.
- [7] M. W. Lo and M.-K. J. Chung, "Lunar Sample Return via the Interplanetary Superhighway," *AIAA/AAS Astrodynamics Specialist Meeting*, No. Paper AIAA 2002-4718, Monterey, California, 2002.
- [8] J. S. Parker and M. W. Lo, "Shoot the Moon 3D," *Advances in the Astronautical Sciences, Astrodynamics* (B. G. Williams, L. A. D'Amario, K. C. Howell, and F. R. Hoots, Eds.), Vol. 123, Part III, Lake Tahoe, California, American Astronautical Society, Univelt Inc., 2005, pp. 2067–2086.
- [9] J. S. Parker, "Families of Low-Energy Lunar Halo Transfers," *Advances in the Astronautical Sciences, Spaceflight Mechanics* (S. R. Vadali, L. A. Cangahuala, J. Paul W. Schumacher, and J. J. Guzman, Eds.), Vol. 124, Part I, Tampa, Florida, American Astronautical Society, Univelt Inc., 2006, pp. 483–502.
- [10] M. Ozimek and K. Howell, "Low-Thrust Transfers in the Earth-Moon System Including Applications to Libration Point Orbits," *Journal of Guidance, Control, and Dynamics*, Vol. 33, March-April 2010, pp. 533–549.
- [11] W. S. Koon, M. W. Lo, J. E. Marsden, and S. D. Ross, "Shoot the Moon," *AAS/AIAA Astrodynamics Specialist Conference*, No. AAS 00-166, Clearwater, Florida, January 23-26 2000.
- [12] J. S. Parker, *Low-Energy Ballistic Lunar Transfers*. PhD Dissertation, University of Colorado at Boulder, Boulder, Colorado, 2007.
- [13] H. Baoyin and C. R. McInnes, "Trajectories to and from the Lagrange Points and the Primary Body Surfaces," *Journal of Guidance, Control, and Dynamics*, Vol. 29, July-August 2006, pp. 998–1003.
- [14] C. Von Kirchbach, H. Zheng, J. Aristoff, J. Kavanagh, B. F. Villac, and M. W. Lo, "Trajectories Leaving a Sphere in the Restricted Three Body Problem," *Advances in the Astronautical Sciences, Spaceflight Mechanics* (D. A. Vallado, M. J. Gabor, and P. N. Desai, Eds.), Vol. 120, Part II, Copper Mountain, Colorado, American Astronautical Society, Univelt Inc., 2005, pp. 1875–1902.
- [15] E. M. Alessi, G. Gómez, and J. J. Masdemont, "Leaving the Moon by Means of Invariant Manifolds of Libration Point Orbits," *Communications in Nonlinear Science and Numerical Simulation*, Vol. 14, December 2009, pp. 4153–4167.
- [16] C. Conley, "Low Energy Transit Orbits in the Restricted Three-Body Problem," *SIAM Journal of Applied Mathematics*, Vol. 16, 1968, pp. 732–746.
- [17] R. L. Anderson and J. S. Parker, "A Survey of Ballistic Transfers to the Lunar Surface," *21st AAS/AIAA Space Flight Mechanics Meeting*, No. AAS 11-278, New Orleans, Louisiana, February 13-17 2011.

- [18] R. W. Easton, "Regularization of Vector Fields by Surgery," *Journal of Differential Equations*, Vol. 10, 1971, pp. 92–99.
- [19] R. McGehee, "Triple Collision in the Collinear Three-Body Problem," *Inventiones Mathematicae*, Vol. 27, 1974, pp. 191–227.
- [20] R. L. Anderson and M. W. Lo, "Virtual Exploration by Computing Global Families of Trajectories with Supercomputers," *Advances in the Astronautical Sciences, Spaceflight Mechanics* (D. A. Vallado, M. J. Gabor, and P. N. Desai, Eds.), Vol. 120, Part II, Copper Mountain, Colorado, American Astronautical Society, Univelt Inc., 2005, pp. 1855–1874.
- [21] V. Szebehely, *Theory of Orbits: The Restricted Problem of Three Bodies*. New York: Academic Press, 1967, pp. 7-41.
- [22] A. Miele, "Theorem of Image Trajectories in the Earth-Moon Space," *Astronautica Acta*, Vol. 6, No. 51, 1960, pp. 225–232.
- [23] G. Gómez, A. Jorba, J. Masdemont, and C. Simó, "Study of the Transfer from the Earth to a Halo Orbit Around the Equilibrium Point  $L_1$ ," *Celestial Mechanics and Dynamical Astronomy*, Vol. 56, August 1993, pp. 541–562.
- [24] P. K. Seidelmann, Ed., *Explanatory Supplement to the Astronomical Almanac*. Sausalito, California: University Science Books, 1992.
- [25] W. M. Folkner, J. G. Williams, and D. H. Boggs, "The Planetary and Lunar Ephemeris DE421," Interoffice Memo IOM 343R-08-003, Jet Propulsion Laboratory, March 31 2008.
- [26] R. B. Roncoli, "Lunar Constants and Models Document," Tech. Rep. JPL D-32296, Jet Propulsion Laboratory, September 23 2005.
- [27] "NASA's Exploration Systems Architecture Study," Tech. Rep. NASA-TM-2005-214062, National Aeronautics and Space Administration, November 2005.